Journal of Environmental Chemical Engineering 10 (2022) 108075

Contents lists available at ScienceDirect

Journal of Environmental Chemical Engineering

journal homepage: www.elsevier.com/locate/jece

Degradation of diclofenac aqueous solutions in a 3D electrolytic reactor using carbon-based materials as pseudo third electrodes in fluidized bed, anodic and cathodic configurations

Jawer David Acuña-Bedoya [a,b,*], Christian E. Alvarez-Pugliese [a,e], Samir Fernando Castilla-Acevedo [c,d], Juan J. Bravo-Suárez [c], Nilson Marriaga-Cabrales [a]

[a] Department of Chemical Engineering, Universidad del Valle, Calle 13 # 100–00, Cali 76001, Colombia
[b] Faculty of Chemical Sciences, Universidad Autónoma de Nuevo León, Ciudad Universitaria, Av. Universidad s/n. C. P., 66455 Nuevo León, Mexico
[c] Center for Environmentally Beneficial Catalysis and Chemical & Petroleum Engineering Department, The University of Kansas, Lawrence, KS 66047, United States
[d] Natural and Exact sciences department, Universidad de la Costa, Calle 58 #55 – 66, 080002 Barranquilla, Colombia
[e] Chemical and Electrochemical Technology and Innovation Laboratory, Department of Chemical Engineering, Texas Tech University, Lubbock, TX 49709, United States

ARTICLE INFO

Editor: Despo Fatta-Kassinos

Keywords:
Boron doped diamond
Electro-oxidation
Adsorption
Granular activated carbon
Granular expanded graphite

ABSTRACT

In this study, the degradation of diclofenac (DCF) in a 3D electrochemical reactor was evaluated. Several parameters were studied including the reactor configuration: fluidized bed (FB), anodic packed bed (APB) and cathodic packed bed (CPB); and the type of pseudo third electrode material: granular activated carbon (GAC) and granular expanded graphite (GEG). The configuration that showed the highest total organic carbon (TOC) removal was the APB, with values up to 85%. In addition, when the substrate saturation of the pseudo third electrode was 20% in the APB, the energy consumption was 2.5 times lower than the conventional 2D reactor. This efficient conversion was the result of improved contacting and reaction between hydroxyl ($HO^{\bullet}$) and sulfate ($SO_4^{\bullet-}$) radicals electro-generated on the anode surface and DCF adsorbed on the particulate carbon. While the degradation efficiency with the 3D CPB reactor was higher than the FB configuration, it was less effective than the 3D APB reactor because of H_2O_2 production in the cathode, which decomposed to generate $HO^{\bullet}$, but only slowly and not sufficiently to oxidize DCF to a significant extent. Furthermore, it was also found that when two 3D APB reactors were connected in series a more significant TOC decrease (98%) and lower energy consumption (4 times) could be achieved than in a single 2D reactor configuration. This result demonstrated that the 3D electrochemical process can be cheaper and faster. All these results highlight the 3D anodic electro-oxidation process as a potential technology to efficiently treat recalcitrant contaminants of emerging concern.

1. Introduction

Diclofenac (DCF) is one of the most globally consumed non-steroidal anti-inflammatory drugs. In many countries, medical prescriptions for DCF are not required, making it a popular and ubiquitous drug for the treatment of musculoskeletal and systemic inflammatory states in humans and animals [1,2]. DCF is also one of the most widely detected chemical compounds in surface water and groundwater. The reasons for this are mainly because of its broad use, incomplete assimilation by humans, the release in urine and feces, and inadequate removal in wastewater plants [1]. Concentrations of DCF higher than 100 ng L^{-1} have been found around the world in places such as Antarctica (1000 ng L^{-1}) [3], Umgeni River system (KwaZulu-Natal, South Africa; 10,000 ng/L) [4], and even Europe (e.g., European groundwaters with concentration values from 2.5 ng/L to 590 ng/L) [5,6]. DCF is known to pose a risk to ecosystems and the environment due to adverse effects on aquatic life such as cytological alterations and lesions to liver, kidney and gills in fishes as well as bioaccumulation in ecosystems and other species [1,7–9]. Therefore, it is of utmost importance to find suitable ways to eliminate such recalcitrant compounds from water matrices.

New wastewater treatment alternatives known as advanced oxidation processes (AOPs) have appeared in the last decades [10], including the Fenton process, heterogeneous photocatalysis, sonochemical reactions, sulfate-radical-based AOPs, electrochemical oxidation, and the

* Corresponding author at: Department of Chemical Engineering, Universidad del Valle, Calle 13 # 100–00, Cali 76001, Colombia.
E-mail address: jawer.acuna@correounivalle.edu.co (J.D. Acuña-Bedoya).

https://doi.org/10.1016/j.jece.2022.108075
Received 31 December 2021; Received in revised form 7 June 2022; Accepted 9 June 2022
Available online 13 June 2022

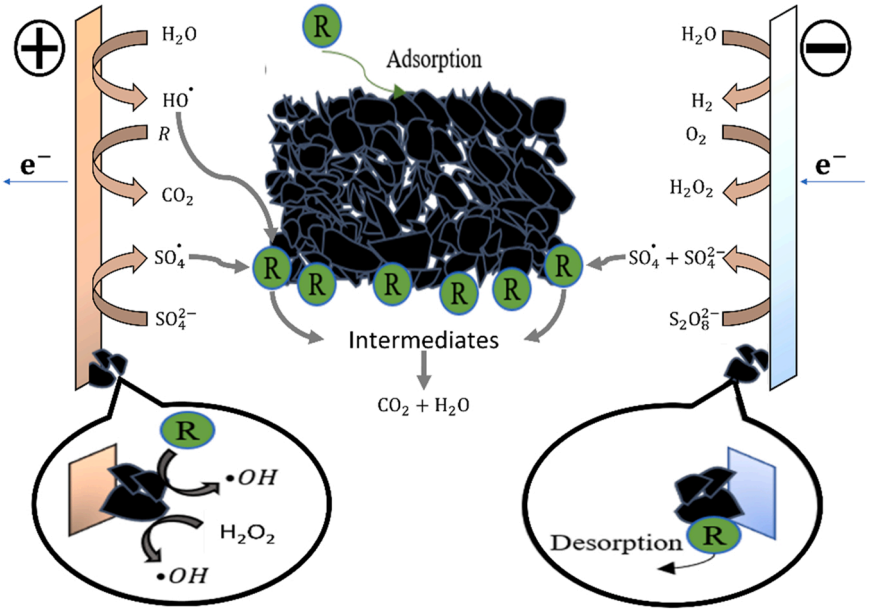

Fig. 1. Schematic representation of the production of hydroxyl and persulfate radicals in the 3D electro-oxidation. A particulate carbonaceous material (pseudo third electrode) in the vicinity of the cathode or anode adsorbs and concentrates substrates (R) which react with radicals towards intermediates and mineralization products.

monochloramine process. AOPs can oxidize organic pollutants due to the formation of potent oxidants such as hydroxyl radicals ($HO^{\bullet}$) (1.8–2.7 V vs NHE), superoxide anions ($O_2^{\bullet-}$) (0.94 V vs NHE), and sulfate radicals ($SO_4^{\bullet-}$) (2.5–3.1 V vs NHE) which facilitate the removal of recalcitrant substances [11–14]. The advantages of AOPs are normally the high mineralization efficiency, high oxidation rates, and no secondary pollution [10]. Among all these AOPs, electrochemical oxidation processes are of great interest. For example, the electro-oxidation using boron-doped diamond (BDD) can operate at ambient temperature and pressure, and with electric power as the primary input. Such characteristics make this technology a potential one for integration as a tertiary process in wastewater treatment plants (WWTP) [15]. More importantly, water can be oxidized in the anode surface of the electrochemical cell to form hydroxyl radicals ($HO^{\bullet}$) (Eq. 1) which can decompose organic compounds (Eq. 2) [16]. Additionally, other powerful oxidants such as sulfate radicals ($SO_4^{\bullet-}$) can be electrogenerated at the BDD anode in wastewater with high sulfate content [17]. Eqs. (3)–(8) below show the generation of $SO_4^{\bullet-}$ at the anode, its reaction with DCF, and secondary reactions to produce persulfate ions and persulfate radicals that also enhance DCF degradation efficiency.

$$BDD + H_2O \rightarrow BDD(HO^{\bullet}) + H^+ + e^- \quad (1)$$

$$BDD(HO^{\bullet}) + R \rightarrow BDD + CO_2 + H_2O + H^+ + e^- \quad (2)$$

$$Na_2SO_4 \rightarrow 2Na^+ + SO_4^{2-} \quad (3)$$

$$SO_4^{2-} + anode \rightarrow anode(SO_4^{\bullet-}) + e^- \quad (4)$$

$$SO_4^{\bullet-} + SO_4^{\bullet-} \rightarrow S_2O_8^{2-} \quad (5)$$

$$S_2O_8^{2-} + anode \rightarrow anode(SO_4^{\bullet-}) + SO_4^{2-} + e^- \quad (6)$$

$$SO_4^{\bullet-} + S_2O_8^{2-} \rightarrow SO_4^{2-} + S_2O_8^{\bullet-} \quad (7)$$

$$SO_4^{\bullet-} + R \rightarrow mCO_2 + SO_4^{2-} + HSO_4^- \quad (8)$$

Although there are reports of complete DCF mineralization by electro-oxidation with BDD electrodes, this process presents drawbacks such as low current efficiency leading to long treatment time, electricity consumption, and limited industrial implementation due to high operating expenses and capital expenditures costs [15,18,19]. One interesting approach that has been explored to overcome current efficiency problems is to add an adsorbent and conducting particulate element as a pseudo third electrode in the electro-oxidation reactor [20–22]. This particulate element, usually made of carbonaceous materials, extends the electrode into the solution, increasing the contact area and improving reactants and products mass transfer. This reactor configuration has been called *a three-dimensional (3D) electrochemical reactor* [23]. The mechanism of organic compounds (R) removal in such 3D electrochemical reactor is presumed to be similar to a 2D system (Fig. S1) except for the role of the particulate electrode which can function as an anodic or cathodic extension and as an adsorbent that preconcentrates the contaminant on its surface [24,25]. As an anodic extension, the generation rate of hydroxyl radicals ($HO^{\bullet}$) from water and sulfate radicals ($SO_4^{\bullet-}$) from sodium sulfate (Na_2SO_4) is expected to increase, thus enhancing the efficiency of pollutants degradation (Eqs. 1–7) [26,27]. Na_2SO_4 was chosen as the electrolyte since it has shown better results than other electrolytes (such as NaCl) in the degradation of organic compounds when BDD anodes are employed [28]. Furthermore, this degradation efficiency is favored at lower current densities, which implies lower costs associated with electricity overcoming present drawbacks in the electro-oxidation with BDD electrodes [15,18]. The general pathway to produce radicals in a 3D electro-oxidation reactor equipped with BDD anodes is schematically shown in Fig. 1.

Different studies have reported the use of 3D electrochemical reactors to degrade different substances. In a previous report, Alvarez-Pugliese et al. studied a 3D electrochemical reactor using: 1) BDD as the anode; 2) stainless steel as the cathode; and 3) a granular activated carbon (GAC) (Calgon, Filtrasorb® 400) packed in the cathodic compartment for DCF treatment as the pseudo third electrode. However, the authors focused on the electrolytic regeneration of the GAC by varying conditions of current density, reaction time, and bed compartment, which led to regenerations of up to 66%. This study also showed that the GAC in contact with the cathode favored its regeneration due to the desorption of the substrate from the carbon surface [29]. Moreover, these authors only studied the CPB configuration which suffers from low efficiencies as it will be demonstrated in the present work.

In a separate report, Pedersen et al. studied the synergistic effect of

the addition of GAC (RESPCARB BRI, 12 ×20 US RGF 3191) on the degradation of different organic pollutants such as 2-methyl-4-chlorophenoxy acetic acid, 2-methyl-4-chlorophenoxy propionic acid, and 2,6-benzamide. Complete degradation was obtained within 1400 min and a synergistic effect (defined as the ratio of pseudo first-order reaction rate constant contribution of the 3D reactor to the sum of 2D reactor and GAC adsorption) of up to 126% was observed [30]. However, this work was performed in a beaker cell operating in a batch configuration which limits its applicability for real-scale conditions.

More recently, Samarghandi et al. studied the degradation of bisphenol A in a 3D electrochemical system operating in batch mode using a graphite/β-PbO_2 anode and GAC (8–10 mesh, Merck Co.) as a particulate electrode placed between the anode and cathode. Different process parameters were varied and the best performance was found to be at a pH of 4.6, electrolyte concentration of 0.074 mol L^{-1}, current density of 35.7 mA cm^2, 25 g of GAC, and 80 min reaction time. Additionally, substrate removals of up to 20% higher than the corresponding 2D electro-oxidation system were achieved, resulting in a synergy of 35% with the particulate electrode [31].

In general, studies have shown that using a 3D electrochemical reactor increases efficiency, making the technology an alternative tertiary treatment in wastewater treatment systems. Different particulate materials can be used in this process, but most of the studies use high surface area porous materials such as GACs, which favor substrate adsorption. However, the rate of adsorption and desorption of organic substances from these materials is usually governed by strong organic-carbon surface interactions and intraparticle diffusion due to the presence of microporosity. These are undesirable properties as they lead to long adsorption and regeneration periods [32]. While carbon materials cost is relatively affordable, they suffer from saturation and surface damage, leading to material losses after subsequent cycles [29,33,34]. Alternatively, other studies have reported the use of non-porous materials with low surface area such as Nyex™. The use of this material significantly reduces the time required to achieve both adsorption equilibrium and electrochemical regeneration, but at the cost of greatly reduced adsorption capacity due to the lack of internal surface area [35, 36]. Clearly, a comparison between carbonaceous materials with high and low porosities and surface areas is needed to determine the effect of the characteristics of related particulate carbon-based materials on a 3D electrochemical process.

To fill this knowledge gap, the present work proposes the use of two different types of commercial porous and non-porous carbonaceous materials: a GAC (Calgon Filtrasorb® 200) and a granular expanded graphite (GEG) (SIGRATHERM® GFG 1200). The latter GEG material has received particular attention in recent decades for its adsorption properties of various organic substances including DCF [37]. In addition, GEG is also an excellent electrical conductor, which is favorable for electrochemical applications requiring improved electrical current transfer [38–40]. Therefore, this study aims to: 1) develop a 3D electrochemical reactor that integrates adsorption-oxidation processes to degrade DCF in aqueous solutions and 2) compare for the first time two carbon materials with different porosities and surface areas to study their effects on the 3D electrochemical process. Moreover, a systematic study will be reported on the variation of operating parameters including reactor configuration, reaction time, current density, and substrate saturation on the carbon pseudo electrode with the aim to improve energy yields and reaction times. The variations of these parameters will allow to discriminate their individual contributions and the relative ability of the various reactor configurations to remove total organic carbon (TOC) in a pollutant sample.

2. Materials and methods

2.1. Particulate material preparation and DCF adsorption

Analytical grade diclofenac (DCF) sodium salt from Sigma-Aldrich® (USA) was used for the adsorption. Commercial GAC Calgon Filtrasorb® 200 (Brazil) and GEG SIGRATHERM® GFG 1200 (Germany) were used as particulate materials whose physical properties are described in Table 1. A physical and thermal pretreatment of crushing, sieving and heating of the carbonaceous materials in an oven at 150 °C for 2 h was carried out before the adsorption tests to eliminate any moisture content.

Table 1
Data of the Characterization of the GAC (FILTRASORB® 200) and GEG (SIGRATHERM® GFG1200) used.

Specifications	Filtrasorb® 200	SIGRATHERM® 1200
Humidity (%)	≤ 2[a]	≤ 5[b]
Particle size (mm)	0.55–0.75 mm[a]	1–1.2[b]
Apparent density (g·L^{-1})	580[a]	200[b]

[a] From Calgon. Carbon data sheet;
[b] From SGL carbon. Material datasheet.

DCF equilibrium adsorption measurements were carried out by contacting 0.1 g of GAC or GEC with 200 mL of DCF solutions of known concentrations over a period of up to 24 h. The beaker containing the solution and carbon samples was placed over a Unimax® 1010 orbital shaker at 250 rpm. Measurements of pH were performed with an Accumet Fischer® pH meter. Small amounts of solution samples were taken every 10 min during the first hour for GAC and every 15 min for GEG, then every hour until the fourth hour and a final sample at 24 h. DCF concentrations of the solution samples were measured by absorption measurements at a wavelength of 276 nm with a Jasco V-730 UV–visible spectrophotometer using a calibration curve based on DCF solutions of known concentrations (Supplementary information, Fig. S2).

2.2. DCF adsorption isotherms

Adsorption isotherms were performed at 25 °C in 250 mL glass beakers for 8 h at five different DCF concentrations of 100, 200, 500, 1000, and 1400 mg_{DCF} L^{-1} with a mass of 0.1 g of GAC or GEG following the procedure described above. Samples were filtered through a 0.45 μm nitrocellulose membrane before being measured, and the solid phase concentrations of the equilibrium adsorbate were calculated from a mass balance. The Langmuir isotherm model (Eq. 9) with the Weber linearization (Eq. 10) were used for equilibrium parameter analysis [41]. In Eqs. (9) and (10), Q_{eq} is the solute concentration retained on the adsorbent (mg g^{-1}), C_f is the concentration of solute in solution (mg L^{-1}) after equilibrium conditions are attained, and Q_o and b are the Langmuir parameters related to the maximum adsorption capacity and the adsorption equilibrium constant, respectively.

$$Q_{eq} = \frac{bQ_0C_f}{1 + bC_f} \tag{9}$$

$$\frac{C_f}{Q_{eq}} = \frac{1}{bQ_0} + \left(\frac{1}{Q_0}\right)C_f \tag{10}$$

The saturation of the carbonaceous material was carried out before each electro-oxidation process, adding 1.4 g of GAC or 0.5 g GEG due to the difference in the apparent densities (580 g L^{-1} for GAC and 200 g L^{-1} for GEG). This process was carried out inside the oxidation cell with the packed particulate material using a solution of 2 L with 125 mg_{DCF} L^{-1} and 0.1 M Na_2SO_4 as shown in Fig. 2. The adsorption time before the electro-oxidation process depends on the total saturation time of each material. Thus, the times to achieve 20% and 100% saturation were evaluated as indicated in Table 2 and these will be used for performance comparison.

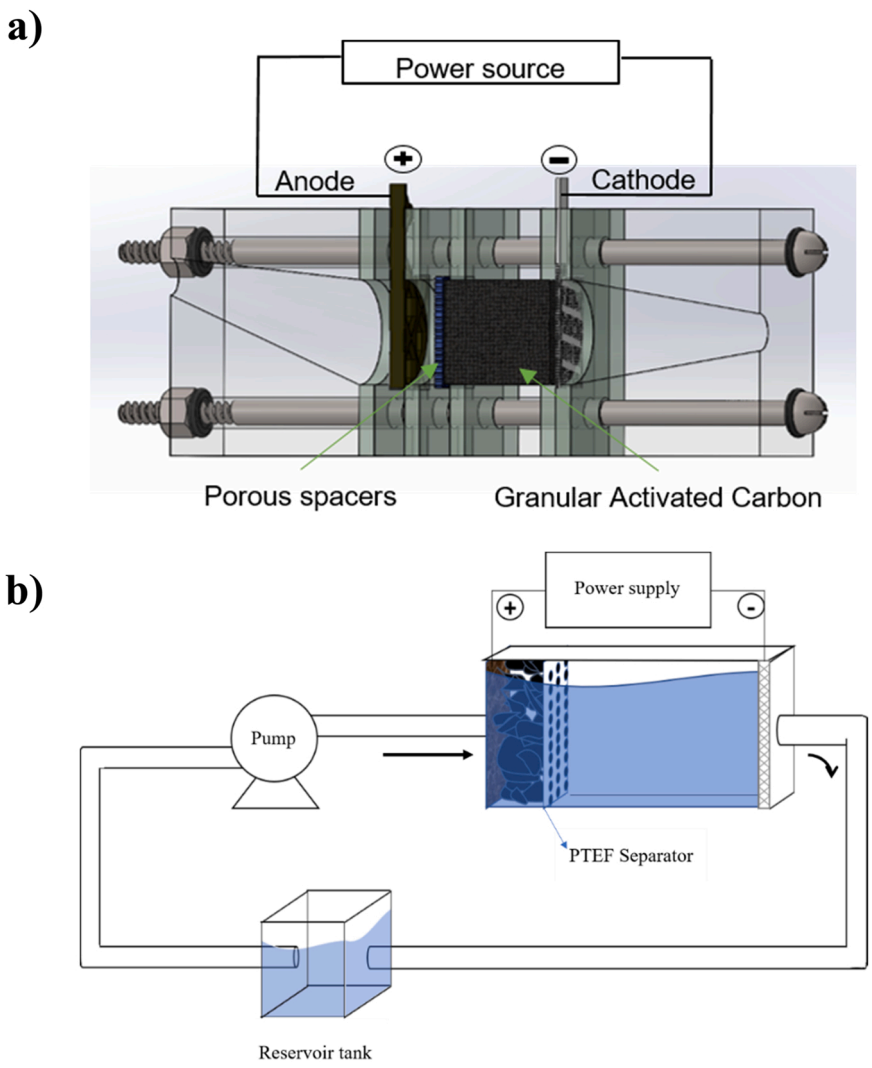

Fig. 2. Experimental setup for the electro-oxidation of DCF: a) Schematics of the electrochemical cell; b) Example of the experimental setup arranged in APB configuration.

Table 2
Adsorption times for the saturation of the carbonaceous materials.

Saturation (%)	Adsorption time (min)	
	GAC	GEG
100	120	360
20	24	72

2.3. Electrochemical oxidation cell

Fig. 2a shows a 27.1 cm^3 polymethyl methacrylate (PMMA) filter press type cell built for the electrochemical oxidation experiments. This design is particularly useful as it can be set up in three different configurations. The first is the fluidized bed (FB) configuration, where the carbonaceous material was suspended between the two electrodes. The second and third are the anodic packed bed (APB) and cathodic packed bed (CPB) configurations, respectively.

In the APB configuration, the carbon material is confined in the anode compartment, whereas in the CPB configuration the carbon material is placed in the cathode compartment. An inert polytetrafluoroethylene (PTFE) mesh (pore size < 500 μm) was placed at 10 mm from the anode or the cathode, depending on the configuration, to ensure confinement of the particulate material in each compartment. The used anode and cathode meshes had a geometric area of 5.3 cm^2. The anode mesh was a commercial BDD (DIACHEM® by CONDIAS®, Germany), whereas the cathode mesh was a stainless steel 304 mesh, which was replaced for each experiment.

2.4. Electro-oxidation with particulate electrode

The 3D anodic electro-oxidation was carried out in the cell described in Section 2.2. and Fig. 2a with the experimental setup shown in Fig. 2b. A peristaltic pump circulated the electrolyte with a flow rate of 137 mL min^{-1} through the cell from a 2 L reservoir tank. The process followed two stages: 1) the concentration of the contaminant (adsorption) and 2) the electro-oxidation of the contaminant. For the first stage, 2 L of 125 mg_{DCF} L^{-1} and 0.1 M Na_2SO_4 solution was circulated through the electrolytic reactor (at open circuit potential) to saturate the particulate material (according to the conditions in Table 2). The second stage started immediately after the adsorption was completed. A current density was applied with a Gamry G750 potentiostat in galvanostatic mode. A SHIMADZU TOC-V series total organic carbon analyzer measured initial and final total organic carbon (TOC). The current densities used were 5, 12.5, and 20 mA cm^{-2} (calculated based on the geometric area of the mesh electrode), and the oxidation times used were 5, 7.5, and 10 h. The carbonaceous material was dried for 24 h in a desiccator before morphological characterization, which was performed

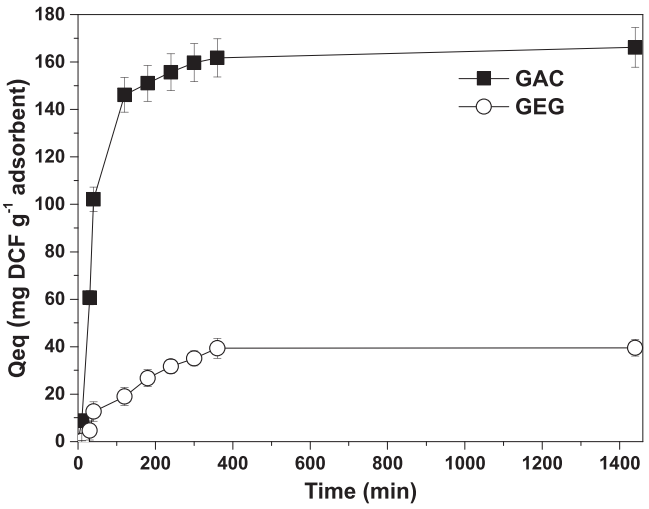

Fig. 3. Temporal DCF equilibrium adsorption tests on GAC and GEG. Experimental conditions: 200 mL solution, 1400 mg_{DCF} L^{-1} (initial DCF concentration), 0.1 g GAC or 0.2 g GEG, 24 h total adsorption time, 250 rpm.

at the beginning and end of each test by scanning electron microscopy (SEM, HITACHI, model SU8230). Additionally, Brunauer–Emmett–Teller (BET) analysis was performed from N_2 physisorption data to determine the specific surface area of each material.

At the end of the DCF degradation process, the particulate material was subjected to the same saturation conditions described in Table 2 to measure its new adsorption capacity. Eq. (11) was used to calculate the regeneration efficiency (RE) of the particulate material at the end of the treatments. Here, RE defines the fraction of adsorption capacity retained in the used particulate material.

$$RE(\%) = \frac{\text{Adsorption capacity of DCF in material after treatment}}{\text{Adsorption capacity of virgin material}} x100 \quad (11)$$

Where adsorption capacities are in $mg_{DCF}\ g^{-1}_{material}$.

2.5. Electric energy per order of magnitude (EEO)

The energy required to reduce the TOC by an order of magnitude (EEO) was calculated to quantify and compare the energy consumption by the different process configurations. These calculations were carried out according to Eq. (12) [42]:

$$E_{EO}\ \left(\frac{kWh}{m^3}\right) = \frac{UJAt}{V \log\left(\frac{TOC_i}{TOC_f}\right)} \quad (12)$$

Where:

U, is the average voltage (*v*).

J, is the current density (mA cm^{-2}).

A, electrode geometric area (cm^2).

t, reaction time (h).

V, reactor volume (m^3).

TOC_i and TOC_f, initial and final substrate carbon concentration (mg L^{-1}).

Finally, after testing each single 3D reactor configuration, an evaluation of a two 3D APB reactors in series was also carried out to determine this configuration's specific energy consumption and for comparison with the single 3D reactors performance.

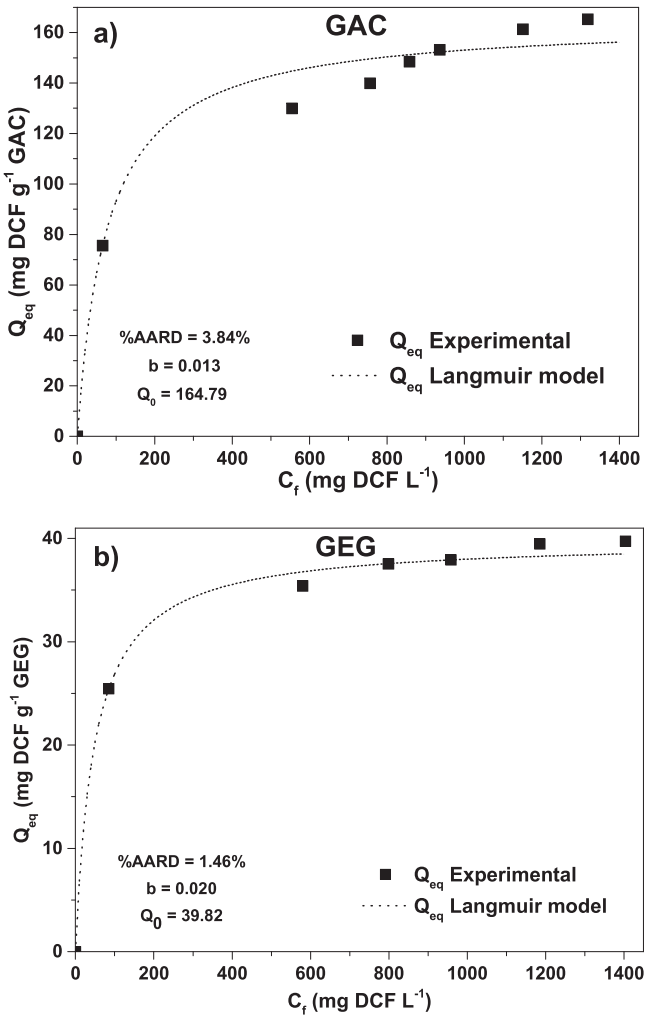

Fig. 4. Experimental DCF adsorption isotherms and Langmuir model ($\mathbf{Q_E = bQ_0C_f/(1+bC_f)}$ fitting for: a) GAC and b) GEG. Experimental conditions: 100–1400 mg_{DCF} L^{-1} (initial concentration), 0.1 g GAC or 0.2 g GEG, 8 h, 24 °C, and 250 rpm.

3. Results and discussion

3.1. Adsorption tests for the carbonaceous materials

Equilibrium adsorption measurements were evaluated for both the GAC and the GEG materials to determine their DCF saturation concentrations. In these experiments, samples of 0.1 g GAC or 0.2 g GEG were kept in solution for 24 h at 25 °C with 1400 mg_{DCF} L^{-1} in 200 mL beakers at 250 rpm. The temporal equilibrium adsorption results are presented in Fig. 3. This figure shows that both carbonaceous materials present different adsorption rates and adsorption capacities for DCF. In the case of GAC, DCF adsorption occurred rapidly within the first 120 min achieving almost 95% of the saturation condition and being almost complete by about 350 min. In the case of GEG near saturation only occurred after 400 min of adsorption. However, the most significant difference was that GAC adsorbed about 4 times more DCF than GEG at equilibrium (160 $mg_{DCF}\ g^{-1}_{GAC}$ vs 40 $mg_{DCF}\ g^{-1}_{GEG}$). The notorious difference in DCF adsorption between DCF in GAC and GEG can be explained by the likely presence of more adsorption sites that can exchange DCF as a result of the significantly higher surface area of GAC (862 $m^2\ g^{-1}$) vs GEG (25 $m^2\ g^{-1}$) [43].

By performing experiments similar to those in Fig. 3, but with varying initial DCF concentrations, the maximum DCF adsorption capacities (Q_0) on GAC and GEG were determined using the non-linearized

and linearized Langmuir model equations (Eqs. 9 and 10). The results in Fig. 4 and S3 show that the Langmuir model leads to a low absolute average relative deviation (%AARD < 3.90%) and also high regression coefficients ($R^2 > 0.985$) for both GAC and GEG samples. This high correlation indicates that the model describes fairly well the adsorption process on both carbon samples and that Langmuir assumptions are valid within the range of the experimental conditions, that is: 1) adsorption occurs in a monolayer with no lateral interactions between adsorbate molecules; 2) adsorption energy is homogeneously distributed in all adsorption sites; and 3) the ability of a molecule to bind to the surface of GAC or GEG is independent of nearby occupied positions [44,45]. These results are in good agreement with those by Lach et al. who studied DCF adsorption with three types of GAC (WG-12, ROW 08 Supra, F-300) at different temperatures and solution pH. These authors also reported high correlation coefficients (R^2) with the Langmuir equation ($0.9699 < R^2 < 0.9921$) [44].

From the Langmuir model and for the GAC sample (Fig. 4a), a maximum adsorption capacity of 164.79 mg_{DCF}/g_{GAC} was obtained. Moreover, the adsorption equilibrium constant was found to be 0.013 L mg_{DCF}^{-1} whereas the separation factor ($R_L=1/(1+bC_{f,0})$) for the different isotherm points varied between 0.05 and 0.43. According to the literature, this is an indication of the favorability of the adsorption equilibrium and is related to the strength of the adsorbate-adsorbent interactions [44]. When it is 0 it indicates irreversible adsorption, when it is 1 it indicates linear adsorption and when it is in the $0 < R_L < 1$ range it corresponds to a favorable adsorption process [46]. Hence, the results indicate that the Filtrasorb® 200 GAC tested in this work has good DCF adsorption performance. These results also agree with Lach et al. study who reported separation factors between 0.02 and 0.36 for DCF adsorption on three types of GACs (WG-12, ROW 08 Supra, F-300), also indicating that DCF adsorption was beneficial at the range of concentrations studied [44]. Other studies on DCF adsorption using a related Filtrasorb® 400 GAC at 24 and 30 °C showed Q_0's of 462 and 329 $mg_{DCF}\ g_{GAC}^{-1}$, respectively [29,47]. The Q_0 obtained for Filtrasorb® 200 GAC is comparable to that of previous studies, but with significant differences probably related to the variation in surface areas but more likely to the different nature of the GACs surface chemical functional groups where DCF adsorbs. Similarly, other DCF adsorption studies on various GACs (e.g., commercial, made from peach seeds, cocoa shells, and olive stones, and carbon nanotubes) also showed Q_0's in the 41–200 $mg_{DCF}\ g_{GAC}^{-1}$ range which are comparatively similar to that for the Filtrasorb® 200 GAC reported here [8,48,49].

For the GEG material (Fig. 4b), a Q_0 of 39.8 $mg_{DCF}\ g_{GEG}^{-1}$ was obtained. This is lower than the value obtained for the GAC but it is not unexpected because of GEG's (SIGRATHERM® GFG 1200) lower surface area (25.3 $m^2\ g^{-1}$) and more limited access of DCF to the lamellar space in the GEG sample. This result indicates that DCF adsorption is likely limited to the external surface of the GEG, on which $HO^{\bullet}$ and other oxidizing agents in solution contact readily the adsorbed pollutant and thus facilitate DCF degradation process in the electrolytic cell [50]. Previous studies have also reported DCF adsorbed on GEG materials. For example, Vedenyapina et al. studied DCF adsorption (400 mg L^{-1}) using a GEG prepared from foundry graphite by a perchloric acid and thermal process. They obtained a Q_0 of 330 $mg_{DCF}\ g_{GEG}^{-1}$ [37]. While our results on the GEG (SIGRATHERM® GFG 1200) are lower than this value, these differences highlight the challenges of comparing different carbon materials in adsorption and catalytic studies because of their surface physicochemical properties can be significantly different due to varying sourced materials, chemical modifications, and pretreatments. In this work, the minimum parameters to compare carbon adsorbent materials were surface areas and pollutant adsorption capacities; however, more in-depth material surface characterizations would be needed to understand the pollutant-surface interactions and fundamental effects on catalytic conversion which are beyond the scope of the current work [8,51–53].

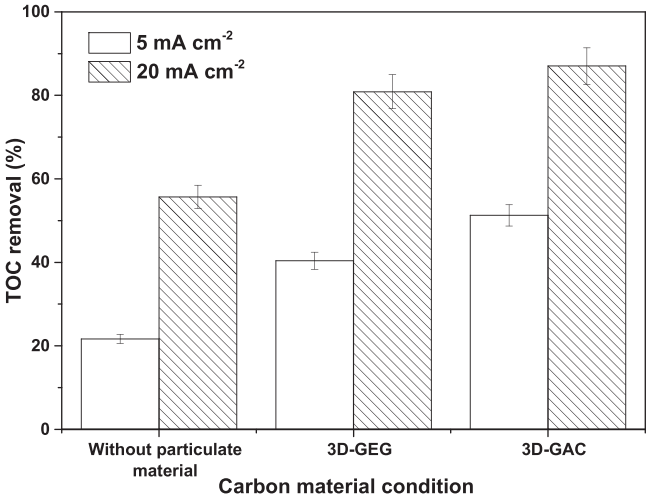

Fig. 5. Effect of the type of carbon material during TOC removal in a 2D and 3D APB reactor configuration. Operational conditions: 25 °C, 5 and 20 mA cm^{-2} current densities, 0.1 M Na_2SO_4 electrolyte, 1.4 g GAC or 0.5 g GEG, 10 h, 20% DCF saturation on GAC and GEG, 125 $mg_{DCF}\ L^{-1}$, 60 $mg_{TOC}\ L^{-1}$.

3.2. Effect of the particulate material source on 2D and 3D electrochemical oxidation

The influence of introducing GAC or GEG materials as a third electrode in the degradation of DCF was also evaluated. For this purpose, the electrochemical tests were performed in the presence and absence of the particulate material using the APB configuration at 25 °C, 5 and 20 mA cm^{-2} current densities, 10 h of treatment, and 20% DCF saturation of the carbonaceous material. The TOC removal results for the 2D and 3D electrochemical processes are shown in Fig. 5. It can be seen that the presence of a pseudo particulate electrode has a positive effect on the degradation of DCF at current densities of 5 and 20 mA cm^{-2} which resulted in corresponding TOC removals of 51.3% and 87% for 3D-GAC and 40.4% and 80.9% for 3D-GEG. These results are higher when compared to the corresponding 21.7% and 55.7% TOC removals found for to the conventional 2D-electro-oxidation without the particulate material. These findings also confirm with other studies where dissolved organic carbon (DOC) removals increased between 15% and 45% for 3D electro-oxidation processes treating organic pollutants such as heavy refinery oils [18], wastewater from the paper industry [54], and formic acid [55].

The DCF degradation process is improved mainly because the particulate material works as an adsorbent for organic compounds. The adsorption allows the pollutant to concentrate on the surface of the GAC or GEG such that $HO^{\bullet}$ radicals formed at the anode have an increased chance of interacting with the DCF on the particulate carbon [56,57]. This additional particulate surface makes the GAC and GEG work as an electrode extension. This extension converts the conventional electrochemical process into a hybrid electrochemical-heterogeneous catalytic oxidation process since $HO^{\bullet}$ radicals can form and/or react on the surface of the carbonaceous materials. Once $HO^{\bullet}$ radicals are formed on the carbon particles or in the vicinity within diffusion distances, the carbon surface can act as an heterogeneous catalyst over which adsorbed pollutants will oxidize following reaction pathways and kinetic models that may resemble multiphasic catalytic reactors [18,58,59].

3.3. Selection of the 3D electrolytic reactor configuration

To select the most suitable reactor configuration and operation conditions for DCF degradation, several experiments were carried out with: 1) three different 3D reactor configurations (FB, CPB, and APB); 2)

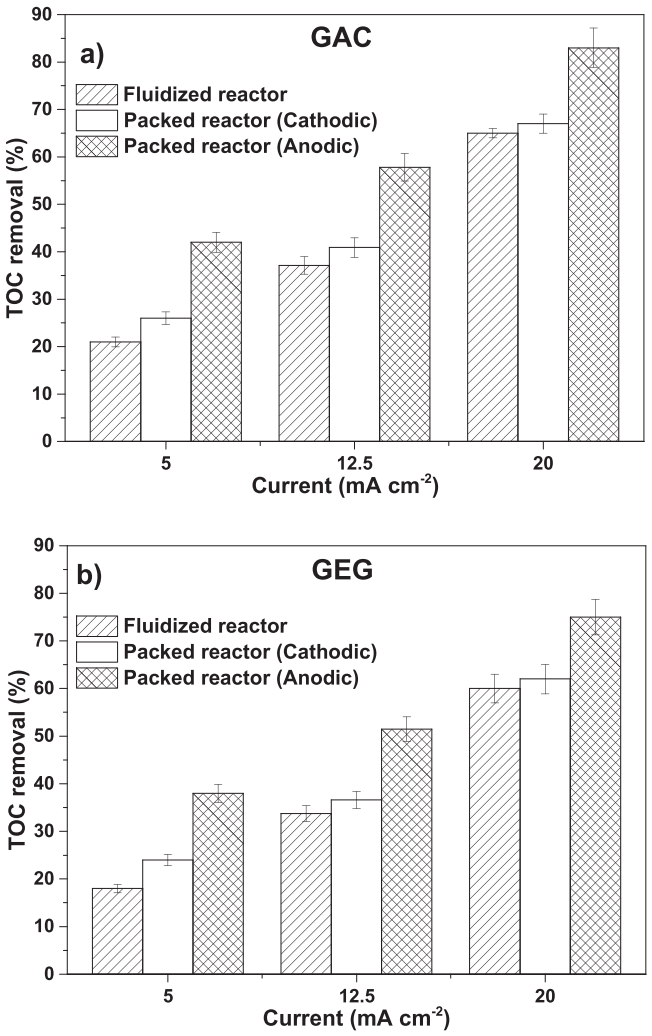

Fig. 6. Effect of the type of reactor on the mineralization of organic matter: a) GAC; b) GEG. Oxidation conditions: Initial concentration 125 mg_{DCF} L^{-1}, current densities of 5, 12.5 and 20 mA cm^{-2}, Na_2SO_4 0.1 M as electrolyte, 25 °C, 1.4 g GAC and 0.5 g GEG, contact time of 10 h, and 100% substrate saturation percentage.

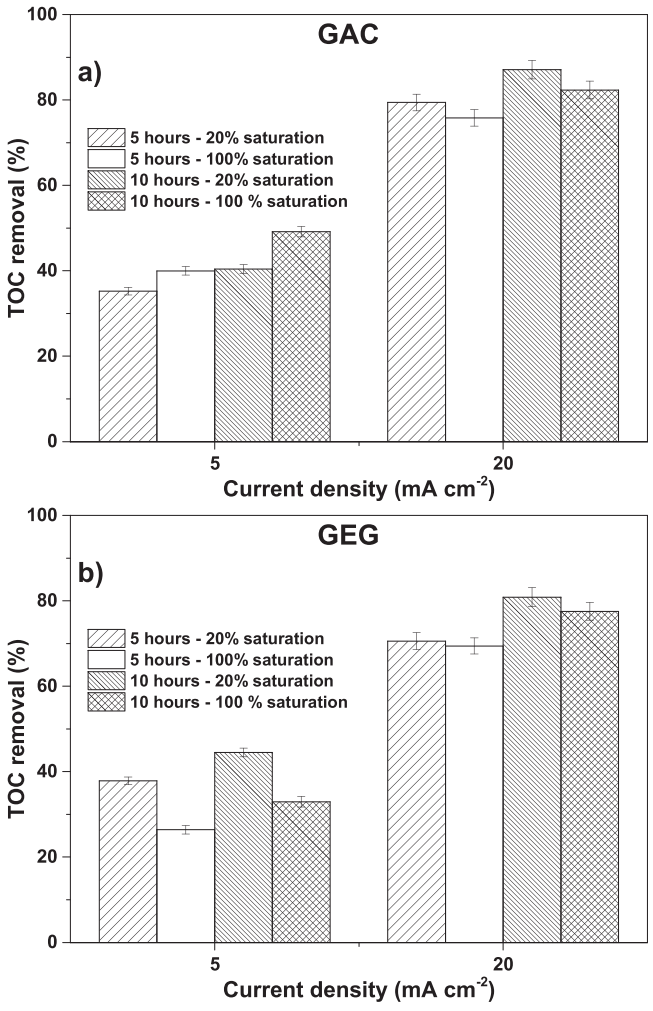

Fig. 7. Effect of current density and DCF degradation time on the total decrease in TOC in a 3D APB reactor configuration: a) GAC and b) GEG. Experimental conditions: 125 mg_{DCF} L^{-1} and 64 mg_{TOC} L^{-1} initial concentrations, 0.1 M Na_2SO_4, 25 °C, 1.4 g GAC or 0.5 g GEG.

three different current densities (5, 12.5, and 20 mA cm^{-2}); and 3) two particulate materials (GAC - Calgon Filtrasorb® 200 and GEG-SIGRATHERM® 1200). Fig. 6a and 6b show the results obtained for the TOC removal using GAC and GEG in the FB, CPB and APB reactors. It was found that the mineralization of DCF in the FB reactor using GAC and GEG was usually 20% lower than those obtained in either of the packed bed reactors, which is expected since the FB reactor does not allow direct contact of all the particulate material with the electrodes. The non-direct contact generates a non-uniform polarization of the particles with bipolar (anodic and cathodic sections within the particles), which negatively influences the efficiency of the process.

The experiments performed on the packed bed reactors show for both materials (GAC and GEG) that the oxidation in the anode compartment was typically 10–17% higher than the CPB or FB configurations. The higher DCF oxidation in the APB configuration is a consequence of the $HO^{\bullet}$ and $SO_4^{\bullet-}$ radicals (by the presence of sulfates in solution) electro-generation on the surface of the anode (Eqs. 1–8) and their reaction with the substrate [34,60]. Therefore, a higher degradation efficiency percent is expected and indeed obtained when the third particulate electrode is in direct contact with the anode instead of the cathode. The DCF degradation percent in the CPB configuration is higher than in the FB configuration since there is production of H_2O_2 on the surface of the cathode from the O_2 reduction reaction which upon decomposition also results in the generation of $HO^{\bullet}$ [61]. However, this decomposition may be slow, lowering the $HO^{\bullet}$ concentration available to oxidize DCF [24,62]. Besides, there is no production of $SO_4^{\bullet-}$ on the cathode surface. The low $HO^{\bullet}$ concentration and lack of production of $SO_4^{\bullet-}$ might be the main reasons why the DCF degradation in the CPB configuration is lower than in the APB configuration. However, it has been reported that the CPB configuration may be advantageous for the desorption of the adsorbed species such as DCF and its degradation products, which facilitates the regeneration of the carbonaceous material [29,60]. Based on the above results, the 3D APB reactor configuration was used for subsequent tests as it resulted in enhanced DCF degradation performance when compared to the 3D CPB and 3D FB reactor configurations.

3.4. Evaluation of operational parameters in the mineralization of DCF

In this section, the effect of the current density, DCF saturation on the carbon material, and the oxidation time were evaluated in the mineralization of a DCF solution containing 125 mg_{DCF} L^{-1} (equivalent to 60 mg_{TOC} L^{-1}) using a 3D APB reactor configuration. The tests were carried out using GAC and GEG with 0.1 M Na_2SO_4 as the electrolyte. Details on the voltages used for each experiment are presented in Table S1. Fig. 7a and 7b show that the TOC removal is proportional to

Table 3
Electric efficiency per order (EEO) and regeneration efficiencies of carbonaceous materials in a 3D APB reactor configuration. Conditions: 5 and 20 mA cm^{-2}, 10 h, 0.1 M Na_2SO_4, 125 mg_{DCF} L^{-1}, 20% DCF saturation.

		GAC	GEG
EEO (kWh m^{-3})			
Current density (mA cm^{-2})	**5**	0.88	0.83
	20	1.07	1.12
Regeneration efficiency (%)			
Saturation (%)	**20**	94.94	40.37
	100	75.28	31.41

the current density and to the time used in the APB configuration for both carbonaceous materials. The main observation is that the highest TOC removals (87% for GAC and 81% for GEG) were achieved using a current density of 20 mA cm^{-2} for 10 h. This is expected since higher current densities lead to a higher concentration of radicals such as $HO^{\bullet}$ and other oxidating species. Higher concentrations of radicals lead to increased degradation rates of DCF into intermediates or CO_2 and water when complete mineralization occurs [46,63–65].

Fig. 7a and 7b also show that at the highest current density (20 mA cm^{-2}) a higher TOC removal was obtained for both carbon materials at the lowest tested saturation percentage (20%). A low saturation percentage suggests that DCF will more likely interact with the carbon most accessible sites [66], which will be mainly present in the macro- and mesopores with average sizes much larger than the average kinetic diameter of DCF [67]. Thus, it is easier for the oxidizing agents to mineralize the pollutants on the surface of the GAC or GEG when the electric current passes through the porous material. The adsorption of DCF in the macro- and mesopores explains why the tests with GAC and GEG have similar TOC removal results as particulate electrodes despite having very different adsorption capacities (Section 3.1). The previous result also suggests that 100% saturation of the adsorbent is not required for efficient DCF removal.

The electric efficiency per order (EEO) was calculated when the DCF saturation on the carbonaceous materials was 20% at both evaluated current densities (5 and 20 mA cm^{-2}) and when the oxidation time was 10 h. The results shown in Table 3 confirm that a current density of 20 mA cm^{-2} is more suitable than 5 mA cm^{-2} from DCF removal and energy consumption points of view. This is the case because it is possible to decrease up to 54% more TOC at the same process conditions with just a smaller percent increase in electrical consumption when using GAC (17%) and GEC (26%) materials. Such increase in current density enhances $HO^{\bullet}$ generation, which leads to a greater DCF mineralization [68,69].

Table 3 shows the calculated EEOs to be around 1 kWh m^{-3}, which are realistic values for practical scale applications since similar technologies such as ozonation (O_3), ozonation and peroxone O_3/H_2O_2, O_3/UV, and UV/H_2O_2 typically operate at EEOs < 1 kWh m^{-3} [70]. The obtained EEO results are also comparable to previous studies that reported almost complete removal of DCF from wastewater by thermal pulsed corona plasma discharge (EEO = 3.8 kWh m^{-3}) [71] and by UV/H_2O_2 (EEO = 0.5 kWh m^{-3}) [72].

The regeneration efficiency (defined as the fraction of adsorption capacity retained in the used material compared to that of the virgin material) is also higher when the initial carbonaceous material saturation is 20% as shown in Table 3. When the adsorbents are fully saturated, organic compounds may adsorb in the micropores of porous materials [67,73]. This affects the oxidation process significantly since the adsorbed organic compounds within micropores cannot be oxidized due to limited spatial (diffusion) access of oxidizing species. Thus, pollutants simply block adsorption sites. Moreover, even when oxidizing species access adsorbed pollutants and react, they can result in polymerized species which may block micropores as they try to diffuse out of the carbon surface. This may be more prevalent when high amounts of contaminants are adsorbed (high surface saturation). In contrast, the

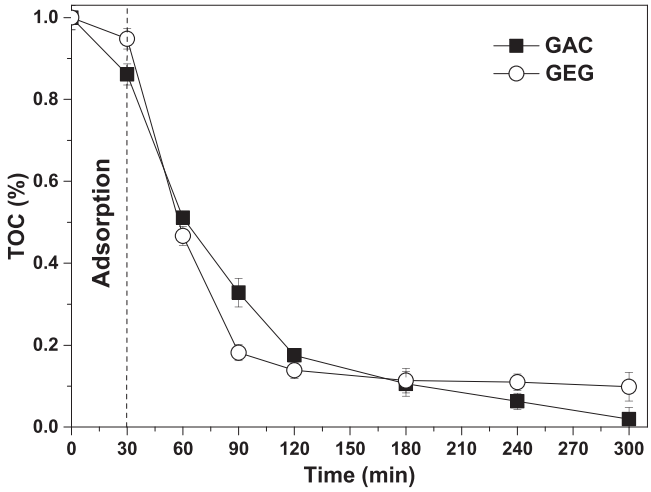

Fig. 8. Performance of the DCF electro-oxidation using two APB reactors in series with GAC and GEG materials. Operational conditions: 5 h, 20% DCF saturation on GAC and GEG, 20 mA cm^{-2}, 0.1 M Na_2SO_4, 25 °C, 1.4 g GAC per cell, 0.6 g GEG per cell, 125 mg_{DCF} L^{-1}, 64 mg_{TOC} L^{-1} TOC as initial concentrations.

oxidation of contaminants on the carbon surface is facilitated when there is a low DCF saturation on the adsorbent. At this saturation level, pores are less likely to get blocked from partially oxidized products diffusing out of the carbon pores, in particular of micropores which are more common in GAC materials [34].

3.5. Performance of the electro-oxidation using two APB reactors in series

Experimental tests using the optimal operating conditions found in the previous section were performed with two APB electrooxidation cells arranged in series. During the first 30 min of the process and in the absence of electric current flowing through the system (dashed line in Fig. 8), it was found that the rate of TOC decrease was much faster with GAC than GEG as a result of the lower DCF adsorption of GEG. Right after 30 min, once the power source was turned on and the current began to flow through the system, the rate of TOC decrease was somewhat comparable, with GEG showing a slightly steeper initial decrease rate than GAC. The initial enhanced rate on GEG can be assigned to the better electric conductivity of GEG compared to GAC, which improves the oxidation process [38–40]. This result also suggests that the heterogeneously catalyzed reaction is limited to the external surface and that GEG may initially form more radicals than the GAC material. However, after 150 min of the process, GEG's rate of TOC decrease plateaued at a value similar to GAC's. This is due to GEG's low DCF adsorption capacity and low concentration of DCF in solution, which decreased the oxidant-DCF interaction. After 150 min, DCF continued to degrade on the GAC material due to its relatively higher adsorption capacity which favored a dynamic DCF adsorption-oxidation process as evidenced in Fig. 8.

In general, Fig. 8 shows that after 5 h (300 min) the TOC removal (%) reached 90% and 98% using GEG and GAC, respectively. This TOC removal represents a value that is around 2.5 times higher than that with just one reactor (described in Section 3.4). These results also indicate that the use of two reactors in series reduces the treatment time due to: 1) doubling of the amount of particulate material and 2) improvements to anode-particulate contact which ultimately lead to more adsorption-oxidation events [60].

When comparisons were done for the electrical energy per order (EEO) for one and two APB reactors configurations with GAC, it was found that to achieve almost complete TOC removal, one single reactor will consume 171% (1.10 kWh m^{-3}) more energy than when using two reactors in series (0.64 kWh m^{-3}). Clearly, the use of two reactors in

Table 4
Surface area, porosity, and regeneration efficiency of the carbonaceous materials before and after the 3D APB reactor electrooxidation process at 20% DCF saturation.

Process step	Surface area (m^2 g^{-1})		Porosity		Regeneration efficiency (%)	
	GAC	GEG	GAC	GEG	GAC	GEG
Initial	862	25.3	0.53	0.12	95	40
Final	431	3.7	0.31	0.03		

series contributes to a reduction of energy consumption of around 42%, mainly attributed to an increase in the efficiency of the adsorption-oxidation process due to improved anode-particulate contact. The EEO results with the two APB reactors in series are even more pronounced when compared with the 2D electro-oxidation process (2.6 kWh m^{-3}) and a single reactor with BDD electrodes (2.54 kWh·m^{-3}) [74]. In summary, the 3D APB electro-oxidation process provided a significant decrease in energy consumption as well as the possibility of regeneration of the carbonaceous material for reuse in the process. Such results are quite encouraging as they indicate that the scaling up of 3D APB reactors in series for DCF mineralization offers not only increases in process throughput but also in energy utilization efficiency.

3.6. *Effect of the process on the particulate matter*

The effect of the electro-oxidation process on the GAC and GEG properties was studied by comparing the BET specific surface areas (SA) and morphology changes (from SEM images) before and after the degradation process (Table 4, Fig. 9). It can be seen from Table 4 that the surface areas for the fresh materials (862 m^2 g^{-1} for GAC and 25.3 m^2 g^{-1} for GEG) are within the expected ranges for typical commercial GACs and GEGs of 800–1100 and 30–40 m^2 g^{-1}, respectively [39,50,63,75]. After the electro-oxidation process, a decrease in surface area of up to 50% for the GAC and 85% for the GEG was observed. These significant area reductions were presumably due to: 1) morphological changes arising from sample attrition (movement generated in the packed bed during liquid pumping) and prolonged contact with the electric current [51,53,76]; and 2) pore clogging from DCF and/or reaction products. These adverse effects lead to changes in the physicochemical properties of pores and surface including variation to functional groups which reduce the efficiency of adsorption, electro-oxidation, and regeneration of the carbon materials [34,53,77].

Fig. 9 shows SEM images of GAC and GEG before (10a and 10c) and after (10b and 10d) the 3D anodic electrooxidation treatment. The GAC images clearly show the presence of irregular surfaces and pores, whereas those for the GEG show smooth, flat, and well-defined surfaces. These results are in agreement with GAC's highly porous and amorphous morphology and with GEG's expected lamellar structure.

After the anodic electro-oxidation process, both materials developed more compact structures presenting large deformities and faults on the surface (Fig. 9b and 9d). Such changes suggest that the 3D electro-oxidation process had a detrimental effect on the integrity of the GAC and GEG. However, these morphological changes are more likely the result of the constant friction of the carbon particles inside the cell during solution recirculation than due to the electrochemistry of the process [78]. One remarkable finding was that, despite the morphological modifications, GAC and GEG material losses were insignificant and only amounted to less than 0.26% regardless of the adsorption times employed. This observation indicates that the reduction in the process time minimized the loss of particulate material. However, the high potentials that arise during the electrochemical cell operation may contribute to the oxidation of GAC and GEG surfaces and to some loss of material [53]. On the other hand, the fractures that appeared in the carbon material may result in the generation of new active or adsorption sites, which help to maintain regeneration efficiencies of up to 95%, despite the reduction in the surface area as a result of micropore blockage [34]. Based on the above results, new research directions could be envisaged, for example, the development of: 1) mesoporous GACs

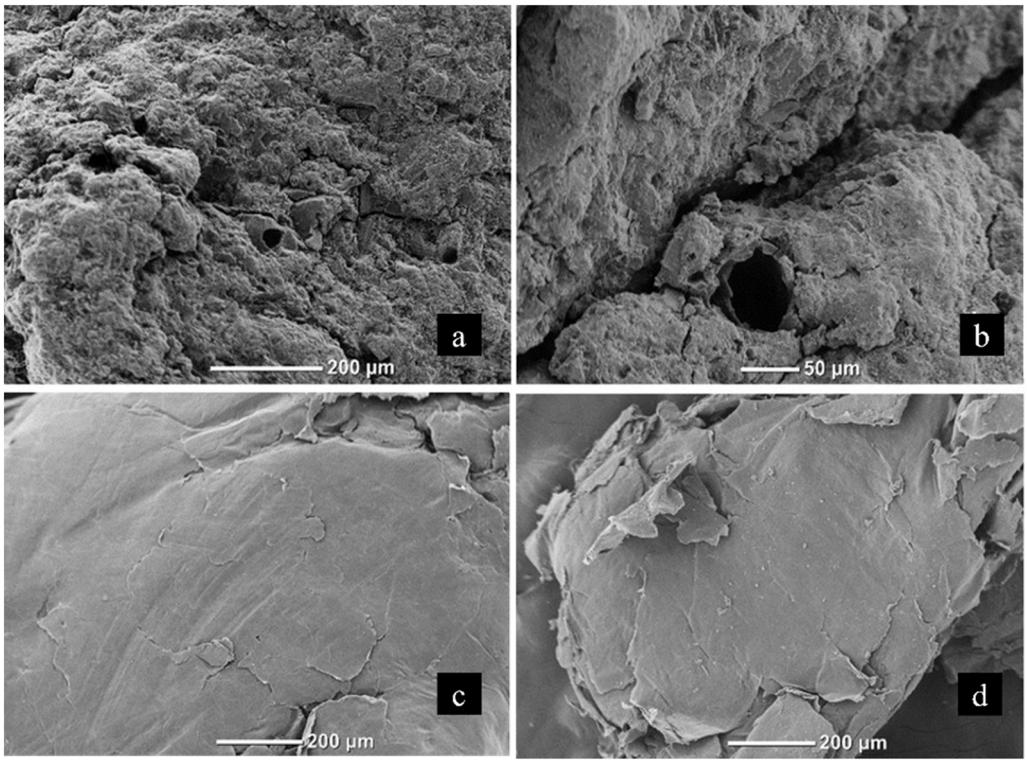

Fig. 9. SEM images of the carbonaceous materials. a) GAC before and b) after anodic electro-oxidation, c) GEG before and d) after anodic electro-oxidation. All images were taken at 100x magnification.

which can allow the diffusion in and out of the pores without major clogging and thus ensuring high surface area utilization; and 2) high surface area or surface modified GEG's to increase pollutants adsorption ability.

4. Conclusions

This work presented a systematic study of the performance of 3D electrochemical reactors in different (FB, APB and CPB) configurations to degrade DCF in dilute aqueous solutions by using carbon materials such as GAC and GEG as pseudo third electrodes. It was demonstrated that the best reactor performance, that is, a high total organic carbon decrease (~85%) and a relatively lower energy consumption could be achieved with a highly porous and amorphous GAC material in a 3D APB reactor. It was also found that more efficient TOC removals (98%) are achievable at shorter treatment times and with even lower energy consumption when two 3D APB reactors were connected in series. More importantly, it was also possible to maintain about 95% of the carbon adsorption capacity for recycle tests by operating the GAC or GEG at DCF saturation levels of around 20% which minimized changes to the carbon surface chemistry. Further mechanistic studies for the 3D anodic electro-oxidation of DCF should provide additional understanding of kinetics and reaction pathways and the potential toxicity of by-products for comparison with the conventional 2D electro-oxidation process. Overall, the results of this work suggest that the use of 3D APB reactors could be an economical alternative to treating water contaminated with emerging contaminants. The introduction of a packed bed particulate material in the electrochemical cell is a relatively easy modification of existing setups and does not require significant infrastructure adjustments. The increased degradation and energy efficiency performances can justify the additional investment and encourage degradation studies of emerging contaminants at the pilot-scale. Of significant interest will be the performance evaluation of this technology in the elimination of pharmaceutical pollutants in the presence of heavy metals, salts, suspended particles, and other interacting organic compounds.

CRediT authorship contribution statement

Jawer David Acuña-Bedoya: Conceptualization, Formal analysis, Investigation, Writing – original draft, Writing – review & editing, Validation, Supervision, **Christian E. Álvarez-Pugliese:**, Writing – review & editing, Visualization, Software, **Samir Fernando Castilla-Acevedo:** Writing – review & editing, **Juan J. Bravo-Suárez:** Writing – review & editing, **Nilson Marriaga-Cabrales:** Methodology, Writing – review & editing, Validation, Supervision, Project Administration, Funding acquisition, Resources.

Declaration of Competing Interest

The authors declare that they have no known competing financial interests or personal relationships that could have appeared to influence the work reported in this paper.

Acknowledgements

The authors would like to thank Minciencias, Colombia for funding the doctoral studies of C.E. Alvarez-Pugliese and the Universidad del Valle, Colombia for funding this research under grant CI – 2917 "Evaluation of alternatives for reducing electricity consumption in the degradation of diclofenac by advanced oxidation processes". J.J.B.-S. acknowledges financial support by the National Science Foundation, United States under grant CBET-1847655.

Appendix A. Supporting information

Supplementary data associated with this article can be found in the online version at doi:10.1016/j.jece.2022.108075.

References

[1] Y. Zhang, S.U. Geißen, C. Gal, Carbamazepine and diclofenac: removal in wastewater treatment plants and occurrence in water bodies, Chemosphere 73 (2008) 1151–1161, https://doi.org/10.1016/j.chemosphere.2008.07.086.
[2] T. Di Lorenzo, M. Cifoni, M. Baratti, G. Pieraccini, W.D. Di Marzio, D.M.P. Galassi, Four scenarios of environmental risk of diclofenac in European groundwater ecosystems, Environ. Pollut. 287 (2021), 117315, https://doi.org/10.1016/j.envpol.2021.117315.
[3] S. González-Alonso, L.M. Merino, S. Esteban, M. López de Alda, D. Barceló, J. J. Durán, J. López-Martínez, J. Aceña, S. Pérez, N. Mastroianni, A. Silva, M. Catalá, Y. Valcárcel, Occurrence of pharmaceutical, recreational and psychotropic drug residues in surface water on the northern Antarctic Peninsula region, Environ. Pollut. 229 (2017) 241–254, https://doi.org/10.1016/j.envpol.2017.05.060.
[4] B.P. Gumbi, B. Moodley, G. Birungi, P.G. Ndungu, Detection and quantification of acidic drug residues in South African surface water using gas chromatography-mass spectrometry, Chemosphere 168 (2017) 1042–1050, https://doi.org/10.1016/j.chemosphere.2016.10.105.
[5] M. Rabiet, A. Togola, F. Brissaud, J.L. Seidel, H. Budzinski, F. Elbaz-Poulichet, Consequences of treated water recycling as regards pharmaceuticals and drugs in surface and ground waters of a medium-sized mediterranean catchment, Environ. Sci. Technol. 40 (2006) 5282–5288, https://doi.org/10.1021/es060528p.
[6] F. Sacher, F.T. Lange, H.J. Brauch, I. Blankenhorn, Pharmaceuticals in groundwaters: analytical methods and results of a monitoring program in Baden-Württemberg, Germany, J. Chromatogr. A. 938 (2001) 199–210, https://doi.org/10.1016/S0021-9673(01)01266-3.
[7] J. Schwaiger, H. Ferling, U. Mallow, H. Wintermayr, R.D. Negele, Toxic effects of the non-steroidal anti-inflammatory drug diclofenac. Part I: Histopathological alterations and bioaccumulation in rainbow trout, Aquat. Toxicol. 68 (2004) 141–150, https://doi.org/10.1016/j.aquatox.2004.03.014.
[8] C. Jung, A. Son, N. Her, K.D. Zoh, J. Cho, Y. Yoon, Removal of endocrine disrupting compounds, pharmaceuticals, and personal care products in water using carbon nanotubes: A review, J. Ind. Eng. Chem. 27 (2015) 1–11, https://doi.org/10.1016/j.jiec.2014.12.035.
[9] E. Brillas, C.A. Martínez-huitle, Decontamination of wastewaters containing synthetic organic dyes by electrochemical methods. An updated review,, Appl. Catal. B, Environ. 166–167 (2015) 603–643, https://doi.org/10.1016/j.apcatb.2014.11.016.
[10] D. Ma, H. Yi, C. Lai, X. Liu, X. Huo, Z. An, L. Li, Y. Fu, B. Li, M. Zhang, L. Qin, S. Liu, L. Yang, Critical review of advanced oxidation processes in organic wastewater treatment, Chemosphere 275 (2021), 130104, https://doi.org/10.1016/j.chemosphere.2021.130104.
[11] V. Satizabal-Gomez, M.A. Collazos-Botero, E.A. Serna-Galvis, R.A. Torres-Palma, J. J. Bravo-Suarez, S.F. Castilla-Acevedo, Effect of the presence of inorganic ions and operational parameters on free cyanide degradation by ultraviolet C activation of persulfate in synthetic mining wastewater, Miner. Eng. 170 (2021), https://doi.org/10.1016/j.mineng.2021.107031.
[12] S.A. Joven-Quintero, S.F. Castilla-Acevedo, L.A. Betancourt-Buitrago, R. Acosta-Herazo, F. Machuca-Martinez, Photocatalytic degradation of cobalt cyanocomplexes in a novel LED photoreactor using TiO<inf>2</inf> supported on borosilicate sheets: a new perspective for mining wastewater treatment, Mater. Sci. Semicond. Process. 110 (2020), https://doi.org/10.1016/j.mssp.2020.104972.
[13] H. Ibargüen-López, B. López-Balanta, L. Betancourt-Buitrago, E.A. Serna-Galvis, R. A. Torres-Palma, F. Machuca-Martínez, S.F. Castilla-Acevedo, Degradation of hexacyanoferrate (III) ion by the coupling of the ultraviolet light and the activation of persulfate at basic pH, J. Environ. Chem. Eng. 9 (2021), 106233, https://doi.org/10.1016/j.jece.2021.106233.
[14] Samir Fernando Castilla-Acevedo, Luis Andrés Betancourt-Buitrago, Dionysios D. Dionysiou, Fiderman Machuca-Martínez, Ultraviolet light-mediated activation of persulfate for the degradation of cobalt cyanocomplexes, J. Hazard. Mater. 392 (2020), https://doi.org/10.1016/j.jhazmat.2020.122389.
[15] F.C. Moreira, R.A.R. Boaventura, E. Brillas, V.J.P. Vilar, Electrochemical advanced oxidation processes: a review on their application to synthetic and real wastewaters, , Appl. Catal. B Environ. 202 (2017) 217–261, https://doi.org/10.1016/j.apcatb.2016.08.037.
[16] T.A. Enache, A.M. Chiorcea-Paquim, O. Fatibello-Filho, A.M. Oliveira-Brett, Hydroxyl radicals electrochemically generated in situ on a boron-doped diamond electrode, Electrochem. Commun. 11 (2009) 1342–1345, https://doi.org/10.1016/j.elecom.2009.04.017.
[17] A. Fernandes, M.J. Nunes, A.S. Rodrigues, M.J. Pacheco, L. Ciríaco, A. Lopes, Electro-persulfate processes for the treatment of complex wastewater matrices: Present and future, Molecules 26 (2021), https://doi.org/10.3390/molecules26164821.
[18] L. Wei, S. Guo, G. Yan, C. Chen, X. Jiang, Electrochemical pretreatment of heavy oil refinery wastewater using a three-dimensional electrode reactor, Electrochim. Acta 55 (2010) 8615–8620, https://doi.org/10.1016/j.electacta.2010.08.011.
[19] J. Zhan, Z. Li, G. Yu, X. Pan, J. Wang, W. Zhu, X. Han, Y. Wang, Enhanced treatment of pharmaceutical wastewater by combining three-dimensional electrochemical process with ozonation to in situ regenerate granular activated carbon particle electrodes, Sep. Purif. Technol. 208 (2019) 12–18, https://doi.org/10.1016/j.seppur.2018.06.030.

[20] M. Zhou, L. Lei, The role of activated carbon on the removal of p-nitrophenol in an integrated three-phase electrochemical reactor, Chemosphere 65 (2006) 1197–1203, https://doi.org/10.1016/j.chemosphere.2006.03.054.
[21] S. Cho, C. Kim, I. Hwang, Electrochemical degradation of ibuprofen using an activated-carbon-based continuous-flow three-dimensional electrode reactor (3DER), Chemosphere 259 (2020), 127382, https://doi.org/10.1016/j.chemosphere.2020.127382.
[22] X. Wu, X. Yang, D. Wu, R. Fu, Feasibility study of using carbon aerogel as particle electrodes for decoloration of RBRX dye solution in a three-dimensional electrode reactor, Chem. Eng. J. 138 (2008) 47–54, https://doi.org/10.1016/j.cej.2007.05.027.
[23] A. Rahmani, M. Leili, A. Seid-mohammadi, A. Shabanloo, A. Ansari, D. Nematollahi, S. Alizadeh, Improved degradation of diuron herbicide and pesticide wastewater treatment in a three-dimensional electrochemical reactor equipped with PbO2 anodes and granular activated carbon particle electrodes, J. Clean. Prod. 322 (2021), 129094, https://doi.org/10.1016/j.jclepro.2021.129094.
[24] R.V. McQuillan, G.W. Stevens, K.A. Mumford, The electrochemical regeneration of granular activated carbons: a review, J. Hazard. Mater. 355 (2018) 34–49, https://doi.org/10.1016/j.jhazmat.2018.04.079.
[25] H. Pourzamani, N. Mengelizadeh, Y. Hajizadeh, H. Mohammadi, Electrochemical degradation of diclofenac using three-dimensional electrode reactor with multi-walled carbon nanotubes, Environ. Sci. Pollut. Res. 25 (2018) 24746–24763, https://doi.org/10.1007/s11356-018-2527-8.
[26] O. Garcia-Rodriguez, E. Mousset, H. Olvera-Vargas, O. Lefebvre, Electrochemical treatment of highly concentrated wastewater: a review of experimental and modeling approaches from lab- to full-scale, Crit. Rev. Environ. Sci. Technol. 52 (2022) 240–309, https://doi.org/10.1080/10643389.2020.1820428.
[27] B.P. Chaplin, Critical review of electrochemical advanced oxidation processes for water treatment applications, Environ. Sci. Process. Impacts 16 (2014) 1182–1203, https://doi.org/10.1039/c3em00679d.
[28] F.L. Guzmán-Duque, R.E. Palma-Goyes, I. González, G. Peñuela, R.A. Torres-Palma, Relationship between anode material, supporting electrolyte and current density during electrochemical degradation of organic compounds in water, J. Hazard. Mater. 278 (2014) 221–226, https://doi.org/10.1016/j.jhazmat.2014.05.076.
[29] C.E. Alvarez-Pugliese, J. Acuña-Bedoya, S. Vivas-Galarza, L.A. Prado-Arce, N. Marriaga-Cabrales, Electrolytic regeneration of granular activated carbon saturated with diclofenac using BDD anodes, Diam. Relat. Mater. 93 (2019) 193–199, https://doi.org/10.1016/j.diamond.2019.02.018.
[30] N.L. Pedersen, M. Nikbakht Fini, P.K. Molnar, J. Muff, Synergy of combined adsorption and electrochemical degradation of aqueous organics by granular activated carbon particulate electrodes, Sep. Purif. Technol. 208 (2019) 51–58, https://doi.org/10.1016/j.seppur.2018.05.023.
[31] M.R. Samarghandi, A. Ansari, A. Dargahi, A. Shabanloo, D. Nematollahi, M. Khazaei, H.Z. Nasab, Y. Vaziri, Enhanced electrocatalytic degradation of bisphenol A by graphite/β-PbO2 anode in a three-dimensional electrochemical reactor, J. Environ. Chem. Eng. 9 (2021), 106072, https://doi.org/10.1016/j.jece.2021.106072.
[32] D. Liu, Water treatment by adsorption and electrochemical regeneration development of a liquid-lift reactor, The University of Manchester, 2015.
[33] J. Acuña-Bedoya, J.A. Comas-Cabrales, C.E. Alvarez-Pugliese, N. Marriaga-Cabrales, Evaluation of electrolytic reactor configuration for the regeneration of granular activated carbon saturated with methylene blue, J. Environ. Chem. Eng. 8 (2020), 104074, https://doi.org/10.1016/j.jece.2020.104074.
[34] O. Garcia-Rodriguez, A. Villot, H. Olvera-Vargas, C. Gerente, Y. Andres, O. Lefebvre, Impact of the saturation level on the electrochemical regeneration of activated carbon in a single sequential reactor, Carbon N. Y 163 (2020) 265–275, https://doi.org/10.1016/j.carbon.2020.02.041.
[35] H.K. Jeswani, H. Gujba, N.W. Brown, E.P.L. Roberts, A. Azapagic, Removal of organic compounds from water: Life cycle environmental impacts and economic costs of the Arvia process compared to granulated activated carbon, J. Clean. Prod. 89 (2015) 203–213, https://doi.org/10.1016/j.jclepro.2014.11.017.
[36] N.W. Brown, E.P.L. Roberts, Combining adsorption with anodic oxidation as an innovative technique for removal and destruction of organics, Water Sci. Technol. 68 (2013) 1216–1222, https://doi.org/10.2166/wst.2013.297.
[37] M.D. Vedenyapina, D.A. Borisova, A.P. Simakova, L.P. Proshina, A.A. Vedenyapin, Adsorption of diclofenac sodium from aqueous solutions on expanded graphite, Solid Fuel Chem. 47 (2013) 59–63, https://doi.org/10.3103/S0361521912060134.
[38] D.M. Nevskaia, A.B. Fuertes, G. Marban, Adsorption of volatile organic compounds by means of activated carbon fibre-based monoliths, Carbon N. Y 41 (2003) 87–96, https://doi.org/10.1016/S0008-6223(02)00274-9.
[39] Y. Wen, K. He, Y. Zhu, F. Han, Y. Xu, I. Matsuda, Y. Ishii, J. Cumings, C. Wang, Expanded graphite as superior anode for sodium-ion batteries, Nat. Commun. 5 (2014) 1–10, https://doi.org/10.1038/ncomms5033.
[40] W. Zheng, S.C. Wong, Electrical conductivity and dielectric properties of PMMA/expanded graphite composites, Compos. Sci. Technol. 63 (2003) 225–235, https://doi.org/10.1016/S0266-3538(02)00201-4.
[41] C.B. Beck, Physicochemical processes for water quality control, Wiley Interscience, John Wiley & Sons, New York, 1973, https://doi.org/10.1002/aic.690190245.
[42] J.R. Bolton, K.G. Bircher, W. Tumas, C.A. Tolman, Figures of merit for the technical development and application of advanced oxidation technologies for both electric and solar driven systems (IUPAC Technical Report), Pure Appl. Chem. 73 (2001) 627–637, https://doi.org/10.1351/pac200173040627.
[43] B.H. Hameed, A.T.M. Din, A.L. Ahmad, Adsorption of methylene blue onto bamboo-based activated carbon: kinetics and equilibrium studies, J. Hazard. Mater. 141 (2007) 819–825, https://doi.org/10.1016/j.jhazmat.2006.07.049.
[44] J. Lach, A. Szymonik, Adsorption of diclofenac sodium from aqueous solutions on commercial activated carbons, Desalin. Water Treat. 186 (2020) 418–429, https://doi.org/10.5004/dwt.2020.25567.
[45] N. González-Ipia, K.C. Bolaños-Chamorro, J.D. Acuña-Bedoya, F. Machuca-Martínez, S.F. Castilla-Acevedo, Enhancement of the adsorption of hexacyanoferrate (III) ion on granular activated carbon by the addition of cations: a promissory application to mining wastewater treatment, J. Environ. Chem. Eng. 8 (2020), 104336, https://doi.org/10.1016/j.jece.2020.104336.
[46] C.J. Sun, L.Z. Sun, X.X. Sun, Graphical evaluation of the favorability of adsorption processes by using conditional langmuir constant, Ind. Eng. Chem. Res. 52 (2013) 14251–14260, https://doi.org/10.1021/ie401571p.
[47] J.L. Sotelo, A.R. Rodríguez, M.M. Mateos, S.D. Hernández, S.A. Torrellas, J. G. Rodríguez, Adsorption of pharmaceutical compounds and an endocrine disruptor from aqueous solutions by carbon materials, J. Environ. Sci. Heal. - Part B Pestic. Food Contam. Agric. Wastes 47 (2012) 640–652, https://doi.org/10.1080/03601234.2012.668462.
[48] C. Saucier, M.A. Adebayo, E.C. Lima, R. Catalu, P.S. Thue, L.D.T. Prola, F. M. Machado, F.A. Pavan, G.L. Dotto, Microwave-assisted activated carbon from cocoa shell as adsorbent for removal of sodium diclofenac and nimesulide from aqueous effluents 289 (2015) 18–27, https://doi.org/10.1016/j.jhazmat.2015.02.026.
[49] S. Larous, A. Meniai, Adsorption of Diclofenac from aqueous solution using activated carbon prepared from olive stones, Int. J. Hydrog. Energy 41 (2016) 10380–10390, https://doi.org/10.1016/j.ijhydene.2016.01.096.
[50] I. Bouaziz, M. Hamza, A. Sellami, R. Abdelhedi, A. Savall, K. Groenen Serrano, New hybrid process combining adsorption on sawdust and electroxidation using a BDD anode for the treatment of dilute wastewater, Sep. Purif. Technol. 175 (2017) 1–8, https://doi.org/10.1016/j.seppur.2016.11.020.
[51] H. Valdés, M. Sánchez-Polo, J. Rivera-Utrilla, C.A. Zaror, Effect of ozone treatment on surface properties of activated carbon, Langmuir 18 (2002) 2111–2116, https://doi.org/10.1021/la010920a.
[52] N. Yuan, A. Zhao, Z. Hu, K. Tan, J. Zhang, Preparation and application of porous materials from coal gasification slag for wastewater treatment: a review, Chemosphere 287 (2022), 132227, https://doi.org/10.1016/j.chemosphere.2021.132227.
[53] H. Valdes, M. Sanchez-Polo, C.A. Zaror, Effect of ozonation on the activated carbon surface chemical properties and on 2-mercaptobenzothiazole adsorption, Lat. Am. Appl. Res. 33 (2003) 219–223.
[54] B. Wang, W. Kong, H. Ma, Electrochemical treatment of paper mill wastewater using three-dimensional electrodes with Ti/Co/SnO2-Sb2O5 anode, J. Hazard. Mater. 146 (2007) 295–301, https://doi.org/10.1016/j.jhazmat.2006.12.031.
[55] A. El-Ghenymy, C. Arias, P.L. Cabot, F. Centellas, J.A. Garrido, R.M. Rodríguez, E. Brillas, Electrochemical incineration of sulfanilic acid at a boron-doped diamond anode, Chemosphere 87 (2012) 1126–1133, https://doi.org/10.1016/j.chemosphere.2012.02.006.
[56] G.W. Reade, A.H. Nahle, P. Bond, J.M. Friedrich, F.C. Walsh, Removal of cupric ions from acidic sulfate solution using reticulated vitreous carbon rotating cylinder electrodes, J. Chem. Technol. Biotechnol. 79 (2004) 935–945, https://doi.org/10.1002/jctb.1076.
[57] K.Y. Foo, B.H. Hameed, A short review of activated carbon assisted electrosorption process: An overview, current stage and future prospects, J. Hazard. Mater. 170 (2009) 552–559, https://doi.org/10.1016/j.jhazmat.2009.05.057.
[58] A. Fortuny, J. Font, A. Fabregat, Wet air oxidation of phenol using active carbon as catalyst, Appl. Catal. B, Environ. 19 (1998), https://doi.org/10.1016/S0926-3373(98)00072-1.
[59] S. Navalon, A. Dhakshinamoorthy, M. Alvaro, H. Garcia, Heterogeneous Fenton catalysts based on activated carbon and related materials, ChemSusChem 4 (2011) 1712–1730, https://doi.org/10.1002/cssc.201100216.
[60] R.V. McQuillan, G.W. Stevens, K.A. Mumford, The electrochemical regeneration of granular activated carbons: a review, J. Hazard. Mater. 355 (2018) 34–49, https://doi.org/10.1016/j.jhazmat.2018.04.079.
[61] W. Zhou, X. Meng, J. Gao, H. Zhao, G. Zhao, J. Ma, Electrochemical regeneration of carbon-based adsorbents: a review of regeneration mechanisms, reactors, and future prospects, Chem. Eng. J. Adv. 5 (2021), 100083, https://doi.org/10.1016/j.ceja.2020.100083.
[62] W. Zhou, X. Meng, Y. Ding, L. Rajic, J. Gao, Y. Qin, A.N. Alshawabkeh, "Self-cleaning" electrochemical regeneration of dye-loaded activated carbon, Electrochem. Commun. 100 (2019) 85–89, https://doi.org/10.1016/j.elecom.2019.01.025.
[63] C.A. Martínez-Huitle, E. Brillas, Decontamination of wastewaters containing synthetic organic dyes by electrochemical methods: a general review, Appl. Catal. B Environ. 87 (2009) 105–145, https://doi.org/10.1016/j.apcatb.2008.09.017.
[64] R. Xie, X. Meng, P. Sun, J. Niu, W. Jiang, Electrochemical oxidation of ofloxacin using a TiO_2-based SnO_2-Sb/polytetrafluoroethylene resin-PbO_2 electrode: Reaction kinetics and mass transfer impact, Appl. Catal. B, Environ. 203 (2017) 515–525, https://doi.org/10.1016/j.apcatb.2016.10.057.
[65] Y. Wang, L. Zhu, N. Ba, F. Gao, H. Xie, Effects of NH4F quantity on N-doping level, photodegradation and photocatalytic H2 production activities of N-doped TiO2 nanotube array films, Mater. Res. Bull. 86 (2017) 268–276, https://doi.org/10.1016/j.materresbull.2016.10.031.
[66] K. Yapsaklı, F. Çeçen, Ö. Aktaş, Z.S. Can, Impact of surface properties of granular activated carbon and preozonation on adsorption and desorption of natural organic

matter, Environ. Eng. Sci. 26 (2009) 489–500, https://doi.org/10.1089/ees.2008.0005.
[67] M. Zhou, L. Lei, The role of activated carbon on the removal of p-nitrophenol in an integrated three-phase electrochemical reactor, Chemosphere 65 (2006) 1197–1203, https://doi.org/10.1016/j.chemosphere.2006.03.054.
[68] C. Comninellis, G. Chen, Electrochemistry for the Enviroment, New York, 2008. http://medcontent.metapress.com/index/A65RM03P4874243N.pdf (accessed March 12, 2014).
[69] E. Brillas, S. Garcia-Segura, M. Skoumal, C. Arias, Electrochemical incineration of diclofenac in neutral aqueous medium by anodic oxidation using Pt and boron-doped diamond anodes, Chemosphere 79 (2010) 605–612, https://doi.org/10.1016/j.chemosphere.2010.03.004.
[70] D.B. Miklos, C. Remy, M. Jekel, K.G. Linden, J.E. Drewes, U. Hübner, Evaluation of advanced oxidation processes for water and wastewater treatment – A critical review, Water Res 139 (2018) 118–131, https://doi.org/10.1016/j.watres.2018.03.042.
[71] N. Nippatlapalli, K. Ramakrishnan, L. Philip, Enhanced degradation of complex organic compounds in wastewater using different novel continuous flow non – Thermal pulsed corona plasma discharge reactors, Environ. Res. 203 (2022), 111807, https://doi.org/10.1016/j.envres.2021.111807.
[72] M. of Environment and climate change, Guidance Document for Integrating UV - based Advanced Oxidation Processes (AOPs) Into Municipal Wastewater Treatment Plants, Showcasing Water Innov. Progr. 28 (2015). ⟨http://civil.engineering.utoronto.ca/wp-content/uploads/2015/09/SWI_Guidance_Document_-_Final.pdf⟩. accessed March 2, 2022.
[73] P. Sathishkumar, R. Viswanathan, Review on the recent improvements in sonochemical and combined sonochemical oxidation processes – A powerful tool for destruction of environmental contaminants, Renew. Sustain. Energy Rev. 55 (2016) 426–454, https://doi.org/10.1016/j.rser.2015.10.139.
[74] G. Coria, J.L. Nava, G. Carreño, Electrooxidation of diclofenac in synthetic pharmaceutical wastewater using an electrochemical reactor equipped with a boron doped diamond electrode, J. Mex. Chem. Soc. 58 (2014) 303–308.
[75] A. Yasmin, J.J. Luo, I.M. Daniel, Processing of expanded graphite reinforced polymer nanocomposites, Compos. Sci. Technol. 66 (2006) 1182–1189, https://doi.org/10.1016/j.compscitech.2005.10.014.
[76] H. Valdés, C.A. Zaror, Heterogeneous and homogeneous catalytic ozonation of benzothiazole promoted by activated carbon: kinetic approach, Chemosphere 65 (2006) 1131–1136, https://doi.org/10.1016/j.chemosphere.2006.04.027.
[77] Z. Ren, D. Zhou, L. Zhang, M. Yu, Z. Wang, Y. Fan, $ZnSn(OH)_6$ Photocatalyst for Methylene Blue Degradation: Electrolyte-Dependent Morphology and Performance, ChemistrySelect (2018) 10849–10856, https://doi.org/10.1002/slct.201802195.
[78] N. Gedam, N.R. Neti, Carbon attrition during continuous electrolysis in carbon bed based three-phase three-dimensional electrode reactor: Treatment of recalcitrant chemical industry wastewater, J. Environ. Chem. Eng. 2 (2014) 1527–1532, https://doi.org/10.1016/j.jece.2014.06.025.